Обзор ArXiv: astro-ph, 1-5 октября 2018

От Сильченко О.К.

ArXiv: 1810.00008

MOSFIRE SPECTROSCOPY OF QUIESCENT GALAXIES AT $1.5 < z < 2.5$.
II. STAR FORMATION HISTORIES AND GALAXY QUENCHING

Sirio Belli[1], Andrew B. Newman[2], Richard S. Ellis[3]

[1]Max-Planck-Institut für Extraterrestrische Physik (MPE), Giessenbachstr. 1, D-85748 Garching, Germany
[2]The Observatories of the Carnegie Institution for Science, 813 Santa Barbara St., Pasadena, CA 91101, USA
[3]Department of Physics and Astronomy, University College London, Gower Place, London WC1E 6BT, UK

ABSTRACT

We investigate the stellar populations for a sample of 24 quiescent galaxies at $1.5 < z < 2.5$ using deep rest-frame optical spectra obtained with Keck MOSFIRE. By fitting templates simultaneously to the spectroscopic and photometric data, and exploring a variety of star formation histories, we obtain robust measurements of median stellar ages and residual levels of star formation. After subtracting the stellar templates, the stacked spectrum reveals the Hα and [N II] emission lines, providing an upper limit on the ongoing star formation rate of $0.9 \pm 0.1\ M_{\odot}$/yr, thus confirming the quiescence of this population. By combining the MOSFIRE data to our sample of Keck LRIS spectra at lower redshift, we analyze in a consistent manner the quiescent population at $1 < z < 2.5$, finding a tight relation between the stellar age and the rest-frame $U-V$ and $V-J$ colors, with a scatter of only 0.13 dex. Using this combined dataset of 79 spectroscopically studied galaxies, we determine an empirical calibration that can be used to estimate the age of quiescent galaxies given their UVJ colors. Applying this age–color relation to large, photometric samples, the number density of quiescent galaxies of various ages can be determined. We model the number density evolution and find evidence for two distinct quenching paths: a fast quenching that produces compact, spheroidal post-starburst systems residing in overdense regions; and a slow quenching of larger galaxies. Fast quenching accounts for about a fifth of the growth of the red sequence at $z \sim 1.4$, and half at $z \sim 2.2$. We conclude that fast quenching is triggered by dramatic events such as gas-rich mergers, while slow quenching is likely caused by a different physical mechanism.

24 галактики: подгонка одновременно спектров и SED

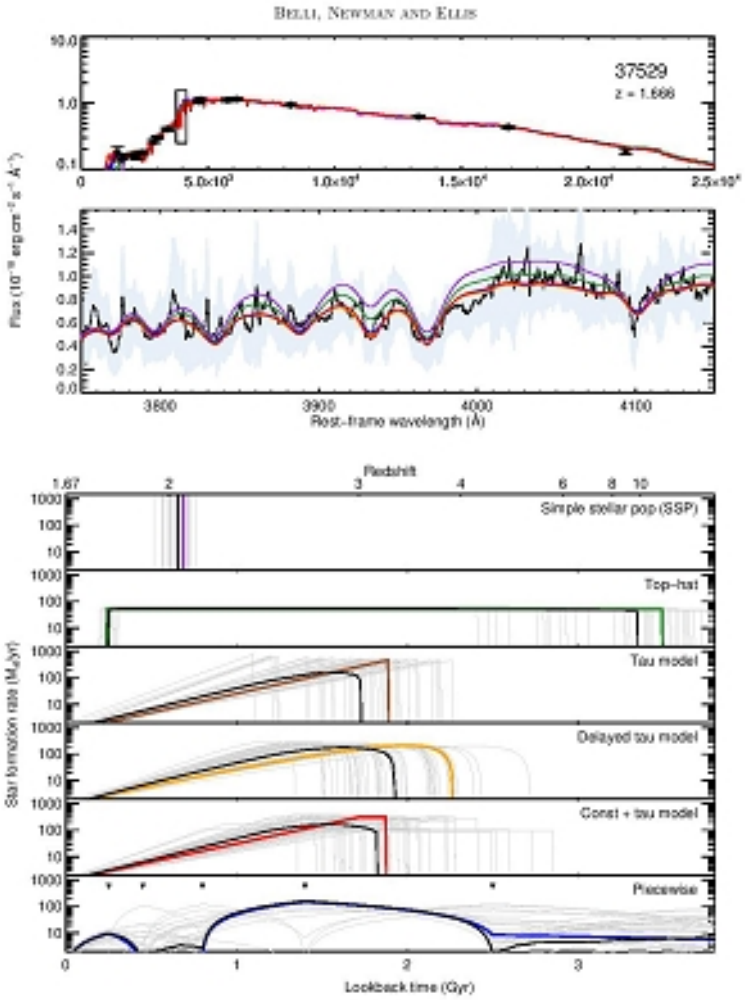

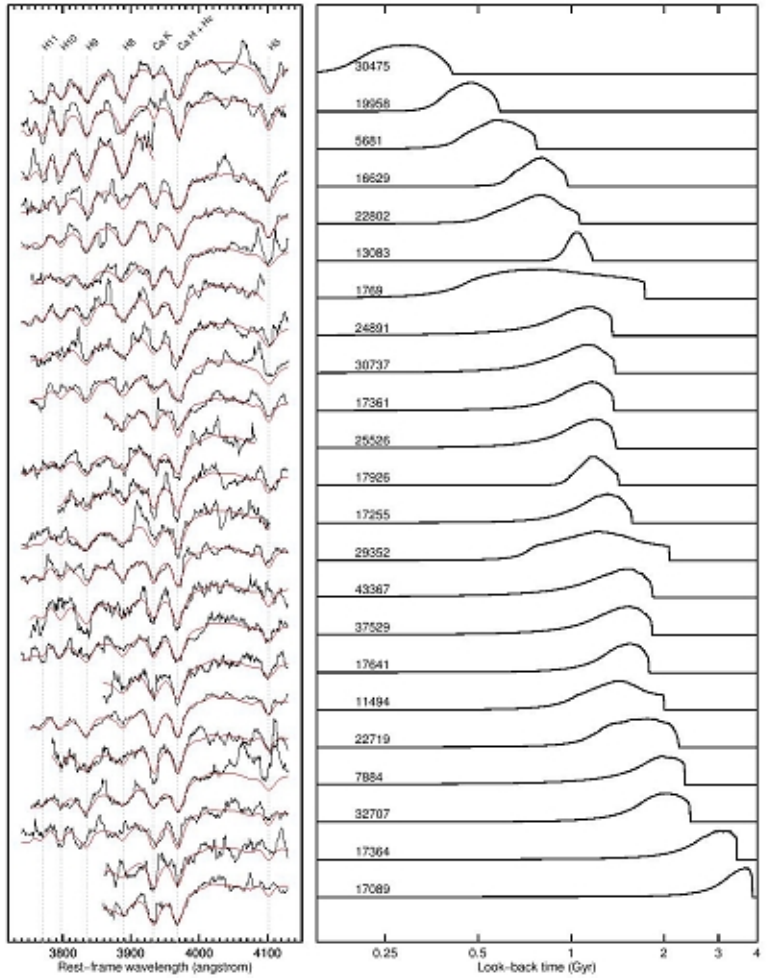

Результат

Table 1. Stellar Population Properties of the MOSFIRE Sample

ID (3D-HST)	Field	z	t_{50}[a] 10^9 yr	A_V[a] mag	Z[a]	log $M_*/M_\odot$[a]	log sSFR[a,b] yr^{-1}	SFR(Hα)[c] $M_\odot$/yr
30475[d]	UDS	1.63	0.30 ± 0.06	0.85 ± 0.10	0.013 ± 0.004	10.71 ± 0.02	-11.0 ± 1.0	< 8.9
19958	COSMOS	1.72	0.48± 0.04	0.73 ± 0.06	0.012 ± 0.002	10.64 ± 0.01	-14.2 ± 3.0	···
5681	COSMOS	2.43	0.61 ± 0.07	0.64 ± 0.09	0.017 ± 0.003	10.91 ± 0.02	-12.9 ± 3.6	< 14.9
16629	COSMOS	1.66	0.81± 0.07	0.44 ± 0.05	0.017 ± 0.003	10.59 ± 0.01	-17.0 ± 5.7	< 7.2
22802	UDS	1.67	0.83 ± 0.1	0.62 ± 0.09	0.015 ± 0.004	11.01 ± 0.02	-13.2 ± 4.9	< 6.8
13083	COSMOS	2.09	1.1 ± 0.1	0.20 ± 0.10	0.022 ± 0.003	10.95 ± 0.03	-20.0 ± 9.8	< 14.5
1769	COSMOS	2.30	1.1 ± 0.2	0.43 ± 0.10	0.022 ± 0.005	11.16 ± 0.03	-11.1 ± 0.2	···
24891	UDS	1.60	1.1 ± 0.1	0.55 ± 0.10	0.015 ± 0.004	10.87 ± 0.02	-10.4 ± 0.09	< 6.3
30737[d]	UDS	1.62	1.1 ± 0.1	0.51 ± 0.09	0.019 ± 0.004	11.23 ± 0.02	-10.6 ± 0.08	< 15.1
17361	COSMOS	1.53	1.1 ± 0.09	0.37 ± 0.07	0.011 ± 0.002	10.74 ± 0.02	-10.9 ± 0.1	< 1.7
25526	EGS	1.75	1.2 ± 0.2	0.34 ± 0.10	0.015 ± 0.005	10.69 ± 0.03	-10.9 ± 1.3	···
17926	EGS	1.57	1.2 ± 0.1	0.33 ± 0.09	0.012 ± 0.002	10.85 ± 0.05	-20.1 ± 10.6	< 2.0
17255	COSMOS	1.74	1.3 ± 0.2	0.31 ± 0.06	0.017 ± 0.004	10.81 ± 0.03	-11.3 ± 0.4	···
29352	UDS	1.69	1.5 ± 0.3	0.23 ± 0.07	0.012 ± 0.003	10.82 ± 0.05	-12.6 ± 5.5	···
43367	UDS	1.62	1.5 ± 0.3	0.68 ± 0.10	0.017 ± 0.004	11.06 ± 0.04	-10.4 ± 0.1	< 9.2
37529	UDS	1.67	1.5 ± 0.2	0.58 ± 0.07	0.014 ± 0.004	10.95 ± 0.04	-10.8 ± 0.08	< 7.9
17641	COSMOS	1.53	1.5 ± 0.2	0.28 ± 0.05	0.013 ± 0.003	10.61 ± 0.04	-11.5 ± 1.8	< 3.0
11494	COSMOS	2.09	1.6 ± 0.2	0.26 ± 0.06	0.022 ± 0.003	11.49 ± 0.03	-11.8 ± 0.09	< 9.9
22719	EGS	1.58	1.8 ± 0.5	0.40 ± 0.09	0.012 ± 0.003	10.96 ± 0.08	-11.7 ± 7.4	< 1.0
7884	COSMOS	2.11	2.0 ± 0.3	0.38 ± 0.06	0.013 ± 0.004	11.35 ± 0.02	-10.7 ± 0.08	< 9.6
32707	UDS	1.65	2.1 ± 0.3	0.31 ± 0.08	0.014 ± 0.004	11.20 ± 0.04	-11.5 ± 0.10	< 13.4
17364	COSMOS	1.53	3.0 ± 0.4	0.13 ± 0.07	0.015 ± 0.003	10.94 ± 0.02	-11.5 ± 0.07	< 1.7
17089	COSMOS	1.53	3.4 ± 0.2	0.30 ± 0.06	0.013 ± 0.002	11.45 ± 0.02	-12.0 ± 0.07	< 2.9

Из-за вырождения параметров модели при варьировании SFH, устойчивыми результатами являются только медианный возраст звездного населения и SFR, осредненная за последние 100 млн лет

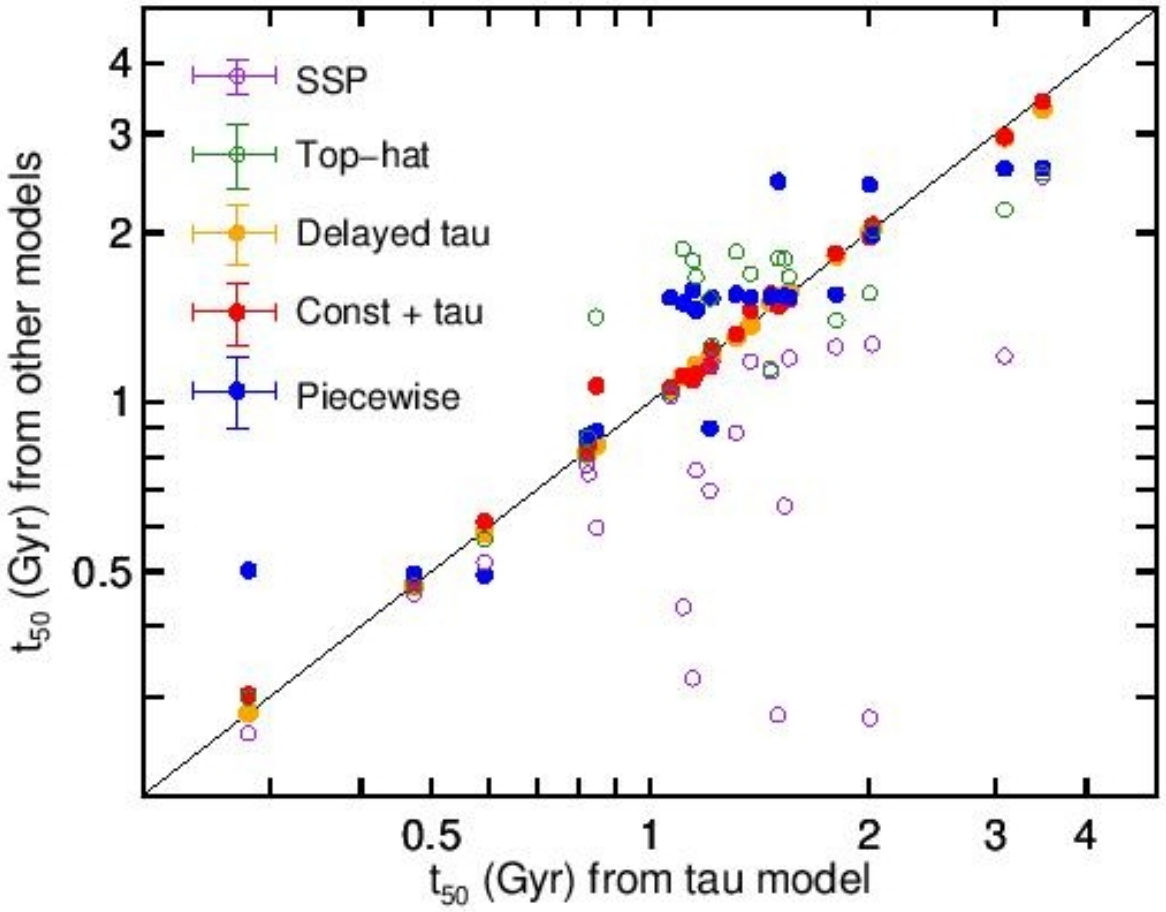

Последовательность возрастов на двухцветной диаграмме?

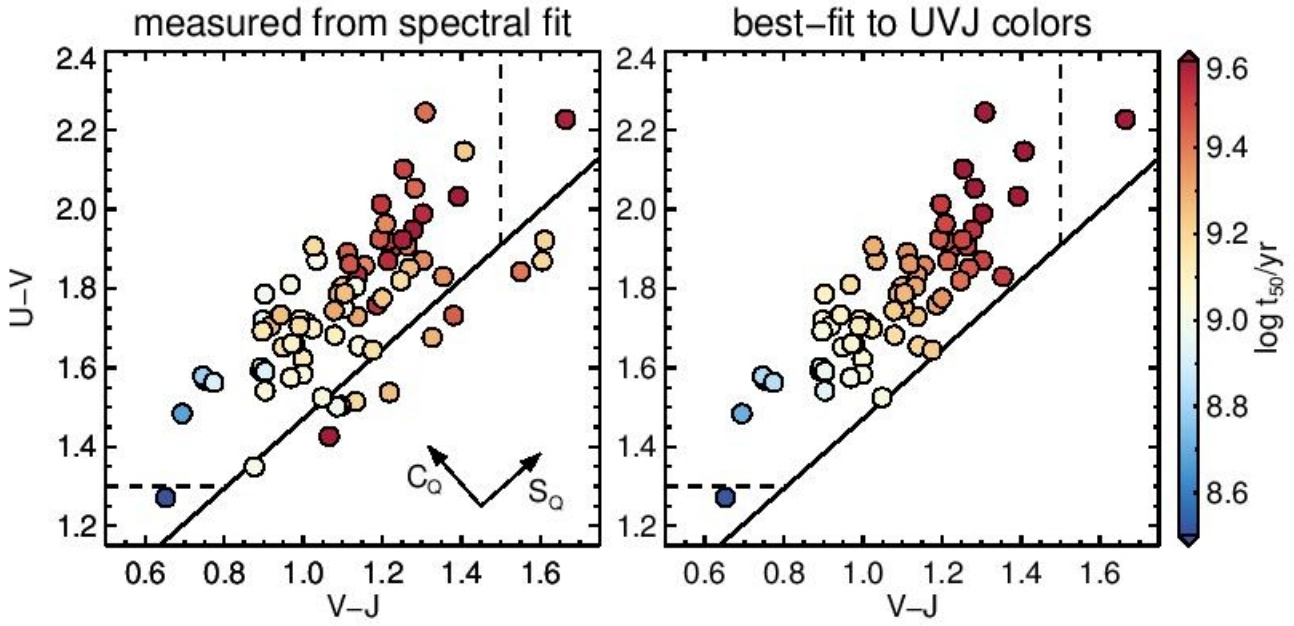

Figure 7. Left: UVJ diagram for both the MOSFIRE and LRIS samples, color-coded by the median stellar age t_{50} as measured from fitting models to the spectroscopic and photometric data. The rotated coordinates S_Q and C_Q are shown in the bottom right corner. Right: same, but color-coded by the median age inferred from the UVJ colors using Equation 3. In this panel only galaxies within the quiescent region, defined by the diagonal black line, are shown. The dashed lines mark the edges of the quiescent population proposed by Muzzin et al. (2013b), which we do not use in our analysis.

Модели подтверждают

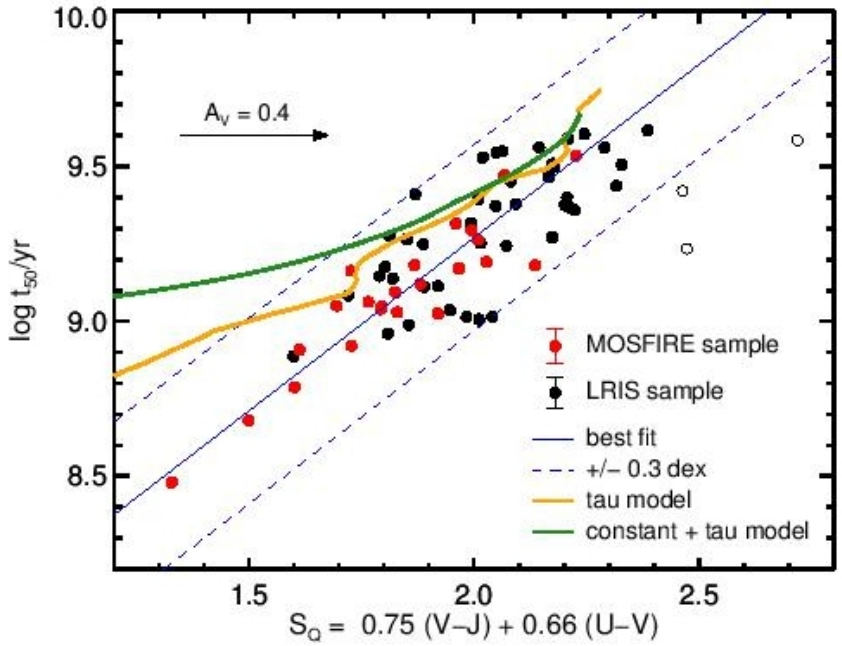

Figure 8. Measured median stellar age as a function of the S_Q coordinate, for both the MOSFIRE (red) and LRIS (black) samples. The median age uncertainties are shown by the error bars in the legend; empty points are outliers and are excluded from the fit. The blue line shows the best-fit given in Equation 3, and the dashed blue lines mark the region within 0.3 dex from the best-fit. The tracks for two simple models of star formation histories are also shown: a tau model with $\tau = 100$ Myr (orange) and a constant star formation of 2 Gyr followed by an exponential decline with $\tau = 100$ Myr (green). The models stop 5.7 Gyr (the age

И вот теперь многотысячная выборка с возрастами по цвету

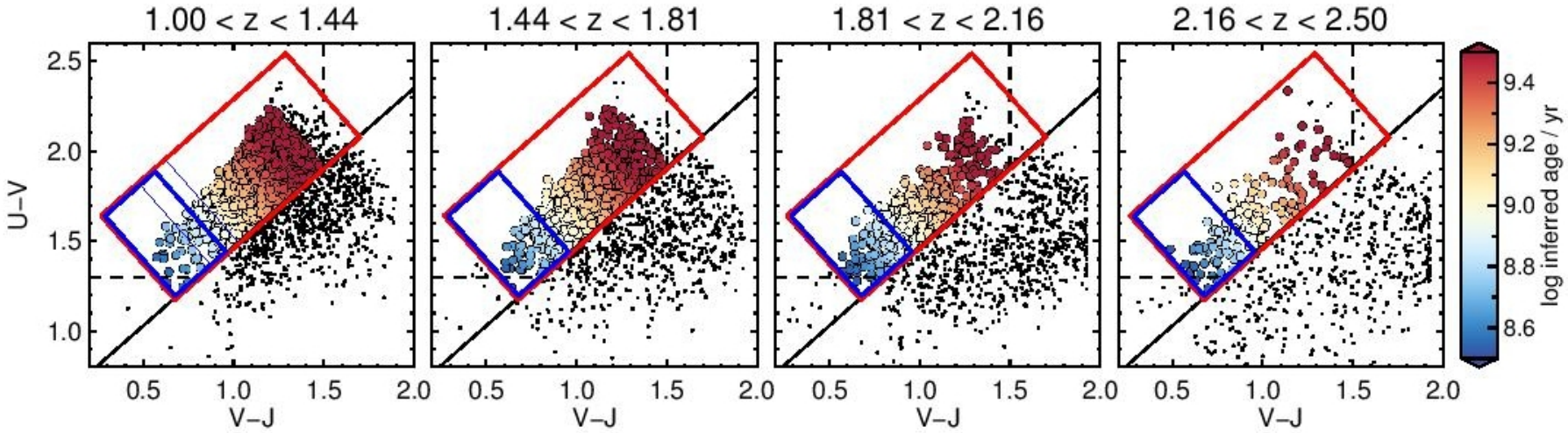

Figure 10. Distribution of the rest-frame UVJ colors for all galaxies with $\log M_*/M_\odot > 10.8$ in the UltraVISTA survey, split into four redshift bins spanning equal comoving volume. The points are color-coded by inferred median ages using Equation 3. Black dots represent galaxies for which the inferred age cannot be calculated, either because they are outside the range in which the age–color relation has been calibrated, or because they are star-forming objects. The red box indicates the selection region for quiescent galaxies; the blue box that for post-starburst galaxies, defined as having 300 Myr $< t_{50} <$ 800 Myr. In the first panel, thin blue lines show how the edge for the selection box changes when adopting a maximum age for post-starburst galaxies of 600 Myr or 1 Gyr.

Попробуем накормить красную последовательность за счет post-starbursts…

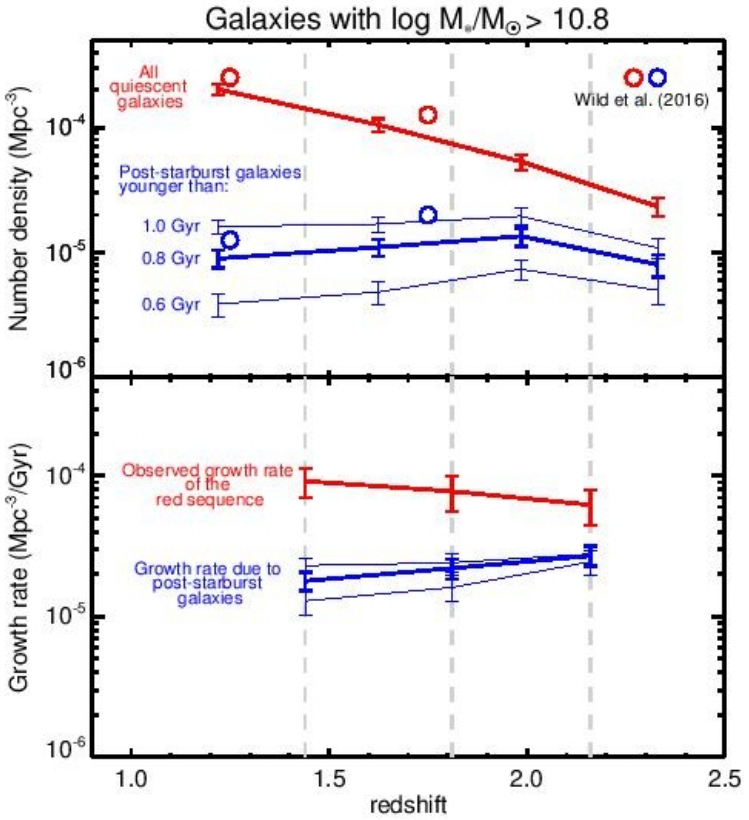

Figure 11. Top: number density of quiescent galaxies (red) and post-starburst galaxies (blue) with $\log M_*/M_\odot > 10.8$ in the UltraVISTA survey. Circles mark the values reported by Wild et al. (2016). Bottom: observed growth rate of the quiescent population (red) and rate of growth due to the flux of post-starburst galaxies (blue). In both panels, the thin blue lines correspond to changes in the threshold age used to select post-starburst galaxies. The vertical dashed lines mark the redshift bins, which are the same as those in

Растить красную последовательность придется пополам за счет быстрой и медленной остановки звездообразования

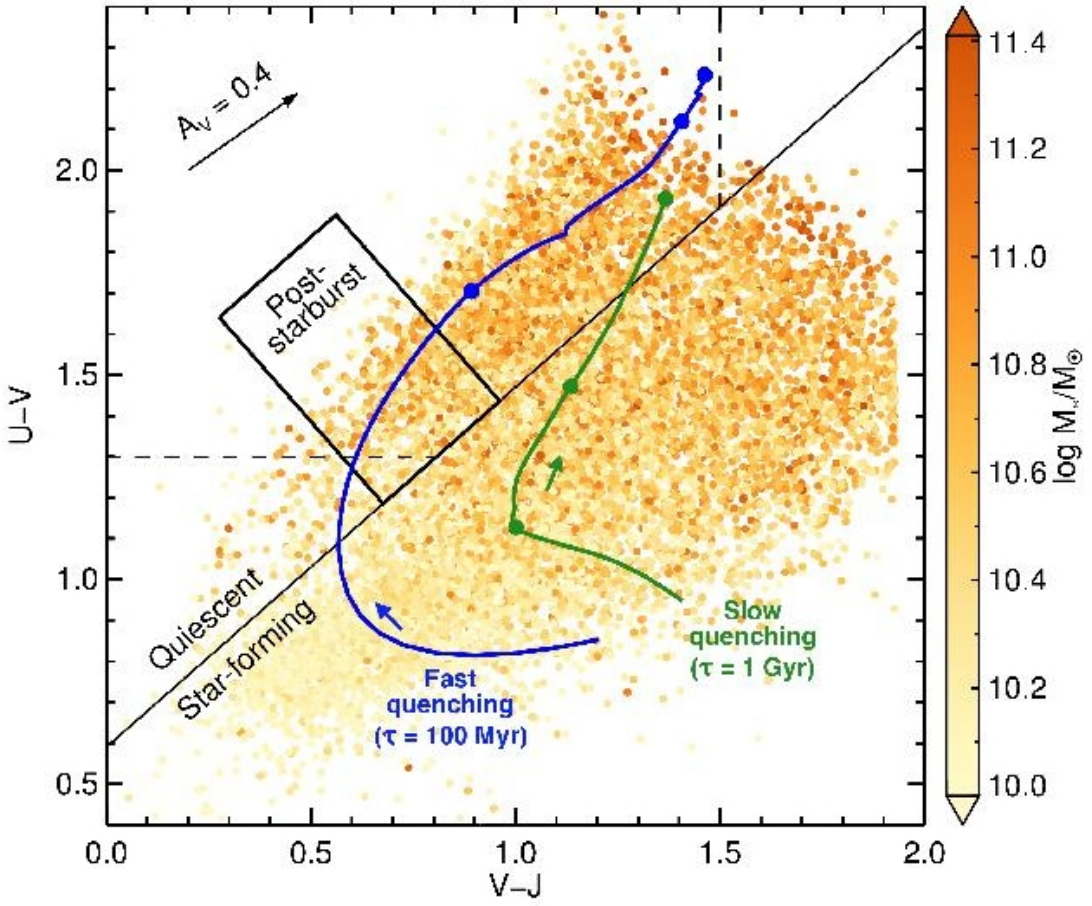

И всякие корреляции…

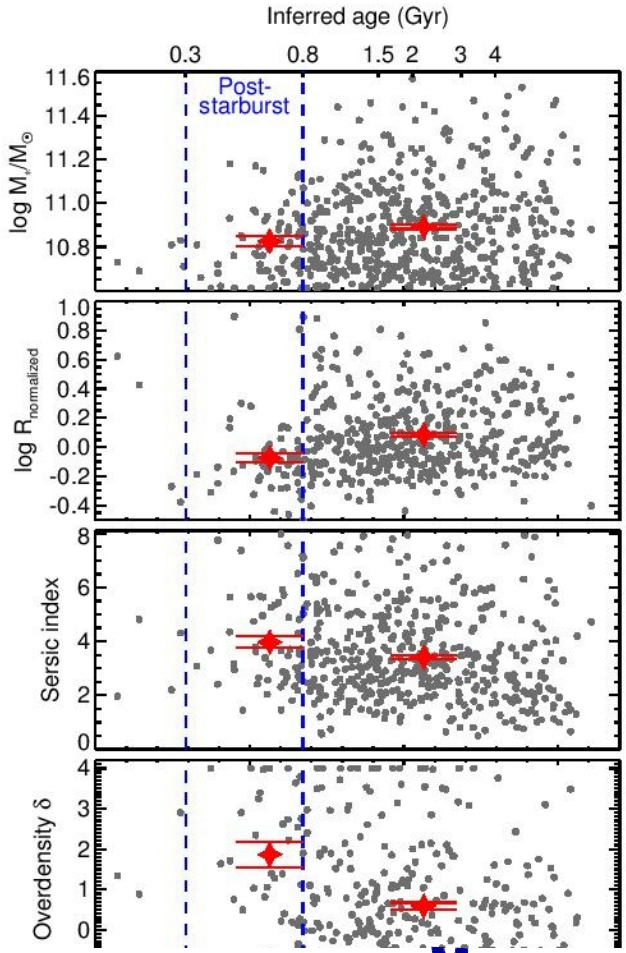

Галактики с «быстрой» остановкой звездообразования

- Меньше массой
- Меньше размером
- Располагаются в плотном окружении

Богатый газом большой мержинг!

ArXiv: 1810.01498

GALAXY STRUCTURE, STELLAR POPULATIONS, AND STAR FORMATION QUENCHING AT $0.6 \lesssim z \lesssim 1.2$

KEUNHO KIM[1], SANGEETA MALHOTRA[2], JAMES E. RHOADS[2], BHAVIN JOSHI[1], IGNACIO FERERRAS[3], AND ANNA PASQUALI[4]

Draft version October 4, 2018

ABSTRACT

We use both photometric and spectroscopic data from the *Hubble Space Telescope* to explore the relationships among 4000 Å break (D4000) strength, colors, stellar masses, and morphology, in a sample of 352 galaxies with $\log(M_*/M_\odot) > 9.44$ at $0.6 \lesssim z \lesssim 1.2$. We have identified authentically quiescent galaxies in the *UVJ* diagram based on their D4000 strengths. This spectroscopic identification is in good agreement with their photometrically-derived specific star formation rates (sSFR). Morphologically, most (that is, 66 out of 68 galaxies, ~ 97 %) of these newly identified quiescent galaxies have a prominent bulge component. However, not all of the bulge-dominated galaxies are quenched. We found that bulge-dominated galaxies show positive correlations among the D4000 strength, stellar mass, and the Sérsic index, while late-type disks do not show such strong positive correlations. Also, bulge-dominated galaxies are clearly separated into two main groups in the parameter space of sSFR vs. stellar mass and stellar surface density within the effective radius, Σ_e, while late-type disks and irregulars only show high sSFR. This split is directly linked to the 'blue cloud' and the 'red sequence' populations, and correlates with the associated central compactness indicated by Σ_e. While star-forming massive late-type disks and irregulars (with D4000 < 1.5 and $\log(M_*/M_\odot) \gtrsim 10.5$) span a stellar mass range comparable to bulge-dominated galaxies, most have systematically lower $\Sigma_e \lesssim 10^9 M_\odot \mathrm{kpc}^{-2}$. This suggests that the presence of a bulge is a necessary but not sufficient requirement for quenching at intermediate redshifts.

Subject headings: galaxies: evolution — galaxies: formation — galaxies: star formation — galaxies: stellar content — galaxies: structure

Фишка работы – глазомерные морфологические типы галактик

Four types of morphology are considered in this work and classified as follows: spheroids satisfying the fractions of $f_{\rm sph} > 2/3$ and $f_{\rm disk} < 2/3$ and $f_{\rm irr} < 0.1$, early-type disks satisfying the fractions of $f_{\rm sph} > 2/3$ and $f_{\rm disk} > 2/3$ and $f_{\rm irr} < 0.1$, late-type disks satisfying the fractions of $f_{\rm sph} < 2/3$ and $f_{\rm disk} > 2/3$ and $f_{\rm irr} < 0.1$, and irregulars satisfying the fractions of $f_{\rm sph} < 2/3$ and $f_{\rm irr} > 0.1$. Additionally, regarding the morphology classification difference between early-type disks and late-type disks, we note that the only difference between the two morphological types is the value of $f_{\rm sph}$. That is, with the same morphological fractions of $f_{\rm disk} > 2/3$ and $f_{\rm irr} < 0.1$, if a galaxy has $f_{\rm sph} > 2/3$ ($< 2/3$), the galaxy is classified as early (late)-type disks. Note our adopted morphological classification differs from the traditional approach that follows the Hubble tuning fork diagram, taking into account the spiral arm structure in late-type systems. Therefore, our definition of early-type disks is more likely to focus on the moderate dominance of both bulge and disk components,

derived value of $\log(M_*/M_\odot) = 9.44$. This stellar mass completeness of $\log(M_*/M_\odot) = 9.44$ reduces our sample size from 996 to 379 galaxies.

Lastly, we apply the morphology classification for our sample of galaxies as described in Section 2.2. Of 379 galaxies, 86, 61, 133, and 72 galaxies are classified as spheroids, early-type disks, late-type disks, and irregulars, respectively. The remaining 27 galaxies do not belong to any of the four morphological types and thus, are excluded from our sample of galaxies. This last sample selection criterion leaves the final sample of 352 galaxies which will be analysed throughout this paper.

Вот по таким изображениям она проводилась…

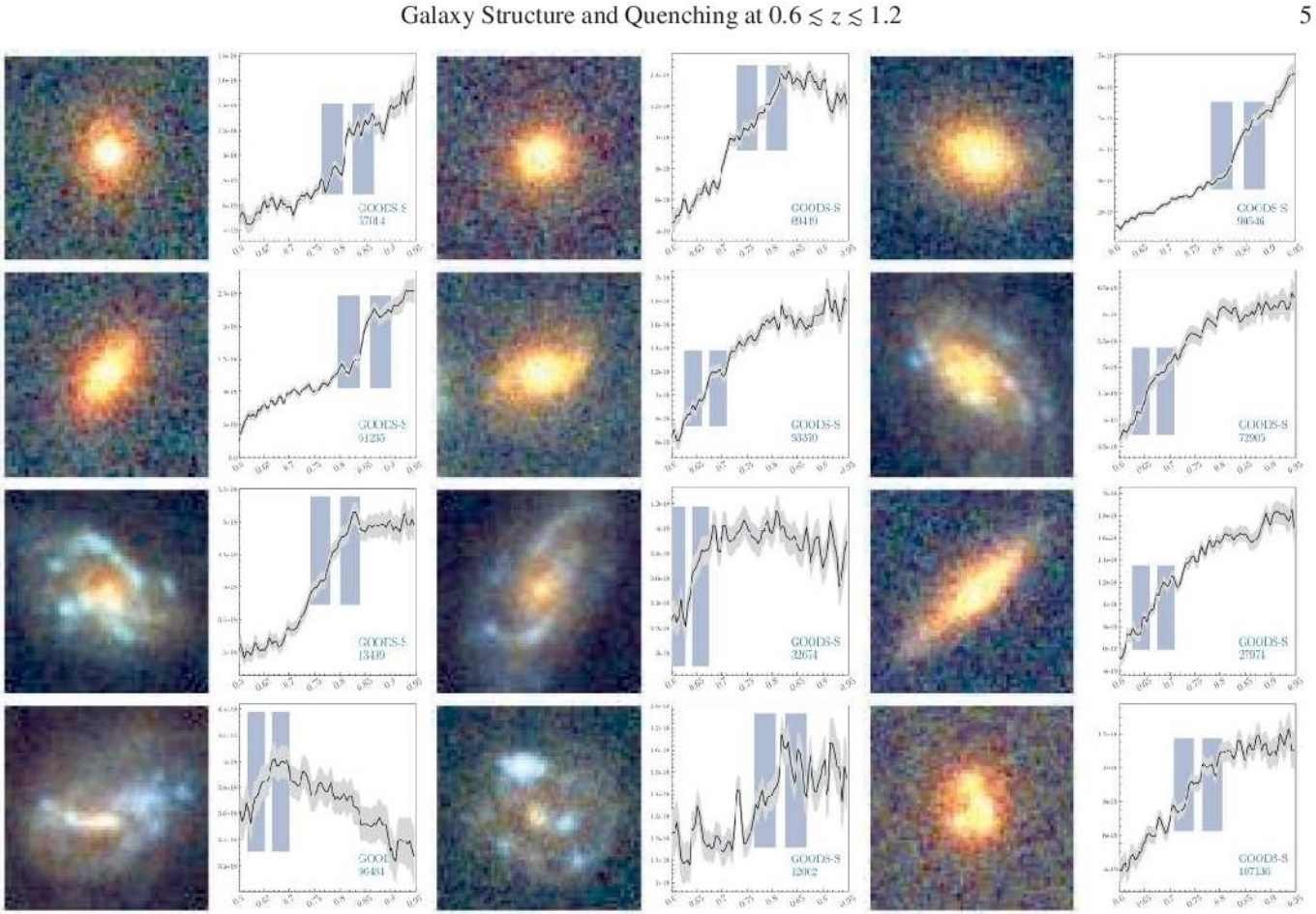

И дальше – уточнение критерия отбора «спокойных» галактик по цвету

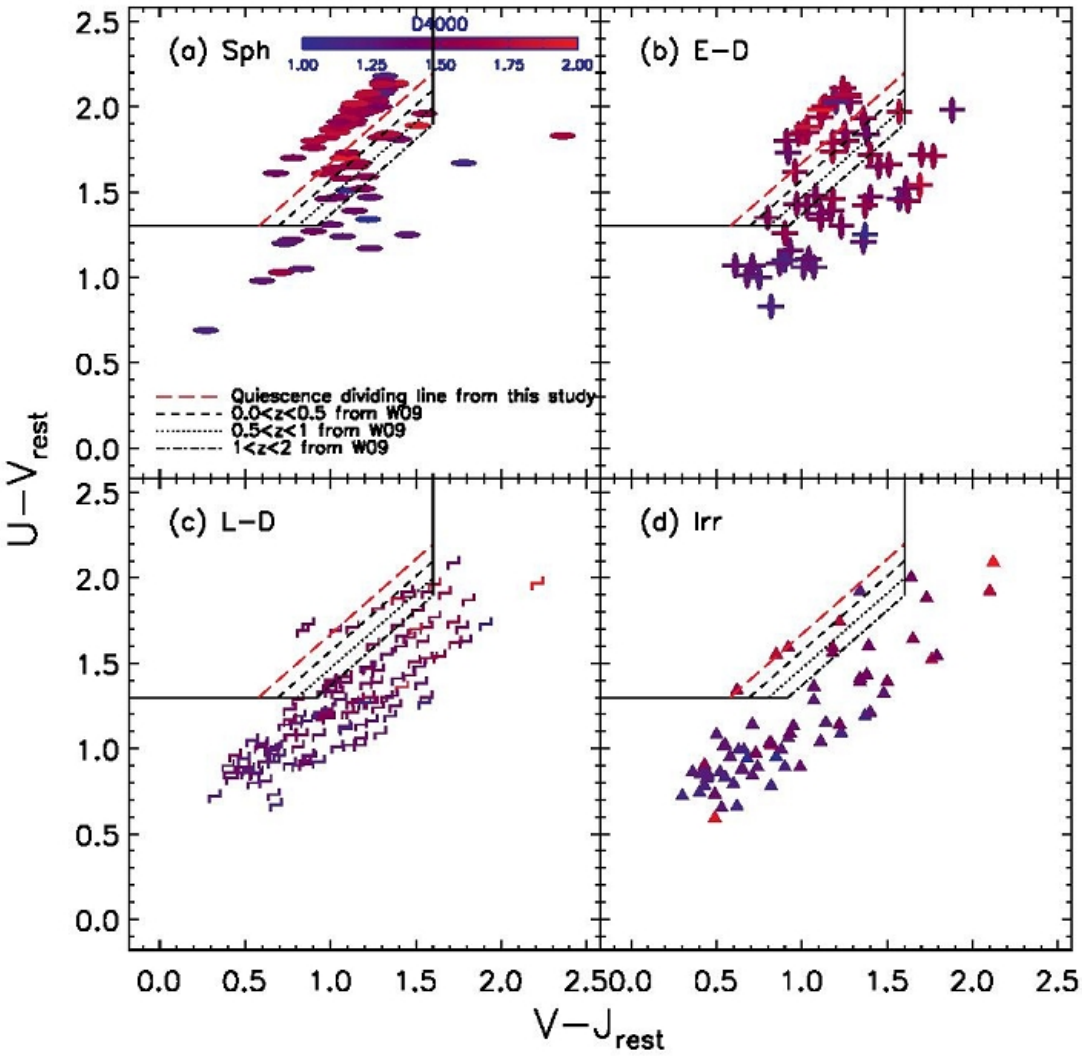

Вроде отобрали…

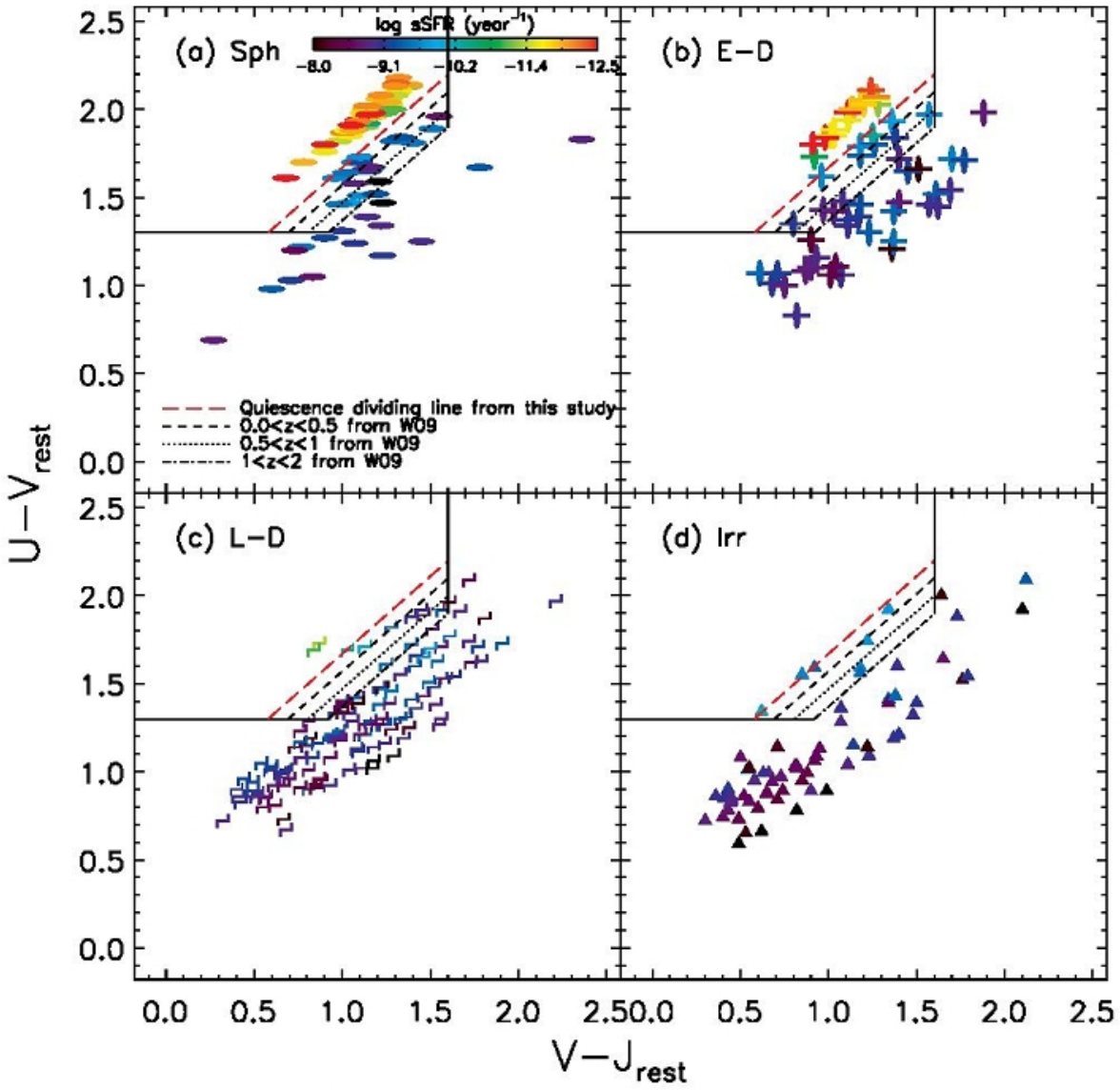

FIG. 4.— The same *UVJ* diagram as Figure 3, but with galaxy specific star formation rate (sSFR). Note that our newly suggested criterion (i.e., the red c line in each panel) for identifying optically quiescent galaxies based on the D4000 strength is qualitatively in good agreement with the distribution of sSF the text for details.

Бимодальность по SF есть у чисто сфероидальных галактик!

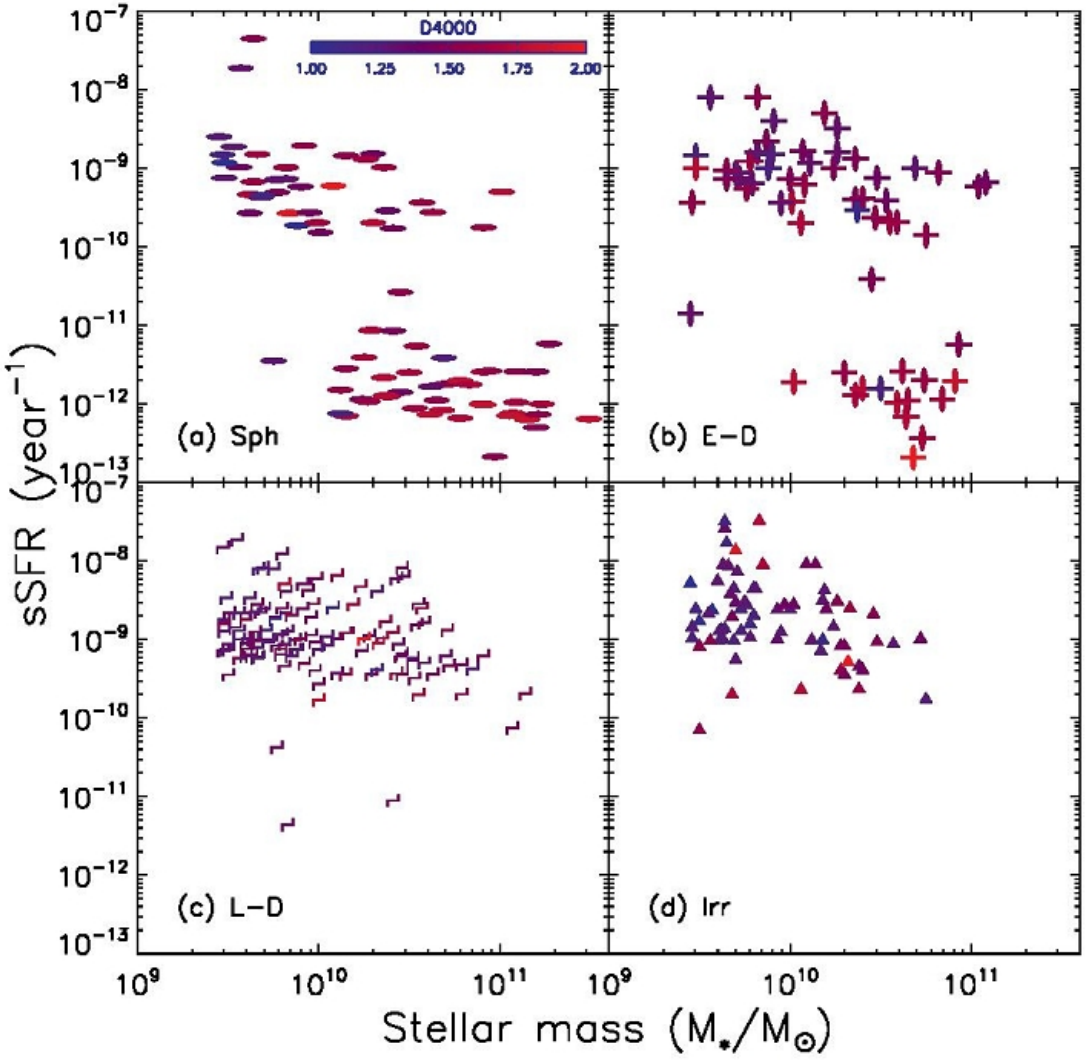

FIG. 7.— sSFR vs. stellar mass with the D4000 strength color-coded. The format is the same as Figure 3. Note that galaxies with a prominent bulge comp
(i.e., spheroids and early-type disks) are separated into two regions depending on their sSFR values, while most of late-type disks and irregulars do not show
remarkable separations. See the text for detail.

ArXiv: 1810.00034

Was the Milky Way a chain galaxy? Using the IGIMF theory to constrain the thin-disk star formation history and mass

Akram Hasani Zonoozi[1⋆], Hamidreza Mahani[1], Pavel Kroupa[2,3],
[1] *Department of Physics, Institute for Advanced Studies in Basic Sciences (IASBS), PO Box 11365-9161, Zanjan, Iran*
[2] *Helmholtz-Institut für Strahlen-und Kernphysik (HISKP), Universität Bonn, Nussallee 14-16, D-53115 Bonn, Germany*
[3] *Charles University in Prague, Faculty of Mathematics and Physics, Astronomical Institute, V Holešovičkách 2, CZ-180 00 Praha 8, Czech Republic*

Accepted .... Received

ABSTRACT

The observed present-day stellar mass function (PDMF) of the solar neighborhood is a mixture of stellar populations born in star-forming events that occurred over the life-time of the thin disk of the Galaxy. Assuming stars form in embedded clusters which have stellar initial mass functions (IMFs) which depend on the metallicity and density of the star-forming gas clumps, the integrated galaxy-wide IMF (IGIMF) can be calculated. The shape of the IGIMF thus depends on the SFR and metallicity. Here, the shape of the PDMF for stars more massive than 1 $M_\odot$ in combination with the mass density in low-mass stars is used to constrain the current star-formation rate (SFR), the star formation history (SFH) and the current stellar plus remnant mass (M_*) in the Galactic thin disk. This yields the current SFR, $\dot{M}_* = 4.1^{+3.1}_{-2.8}\ M_\odot \mathrm{yr}^{-1}$, a declining SFH and $M_* = 2.1^{+3.0}_{-1.5} \times 10^{11} M_\odot$, respectively, with a V-band stellar mass-

Идеи Павла Крупа…

- Все звезды рождаются в скоплениях РАЗНЫХ МАСС;
- А тогда надо складывать не ОДИНАКОВЫЕ солпитеровские функции масс, а сворачивать с функцией масс скоплений, внутри которой защиты вариации верхнего предела масс… Эту свертку Крупа назвал «интегральная галактическая начальная функция масс» (IGIMF)

В принципе, PDMF можно подогнать и чистым «Солпитером»…

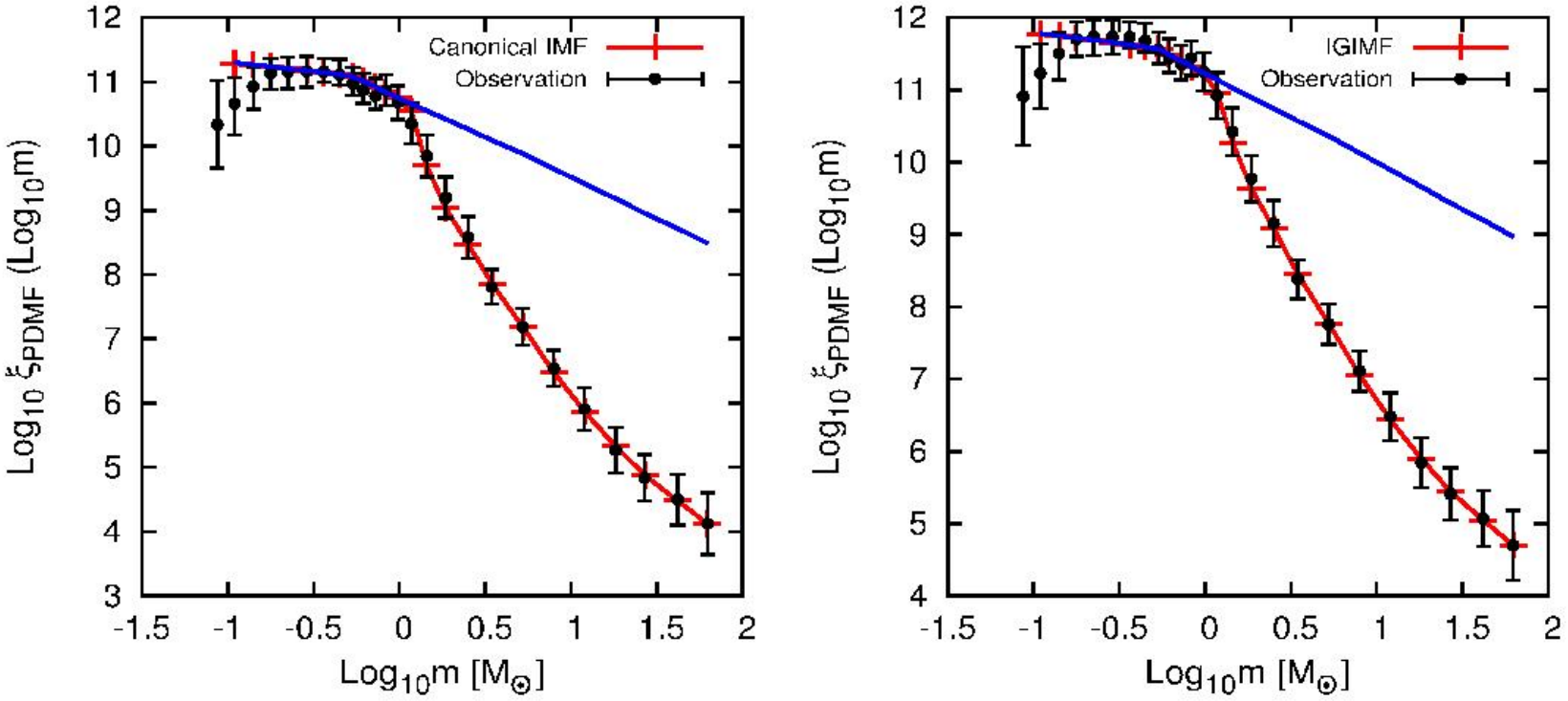

Figure 3. The Milky Way disk PDMF with uncertainties derived by Scalo (1986) is shown as black filled circles. The best-fit models (Fig. 2) are shown as red crosses in both panels. Using the invariant canonical IMF, the best-fitting model has $\tau = 2.8$ Gyr and $M_{tot} = 10^{11} M_{\odot}$. This implies the present-day V-band stellar mass-to-light ratio of the MW to be 1.35. In the case of the IGIMF, the best-fitting model has $\tau = 2.8$ Gyr and $M_{tot} = 4 \times 10^{11} M_{\odot}$ and a V-band mass-to-light ratio of the MW of 2.79. The observed MF is vertically shifted up 9.8 dex to have same number of most massive stars as the modeled PDMF (see footnote 2). In both panels the blue line shows the canonical IMF (Eq. 1) for comparison. The decrease of the observed PDMF below $0.3 M_{\odot}$ stems from using an inappropriate stellar mass-luminosity relation and from not correcting the star-counts for unresolved binary systems (Kroupa et al. 1993), both not known to

Но тогда не будет зависимости PDMF от SFH…

Если опираться не на универсальную IMF, а на «интегральную галактическую»…

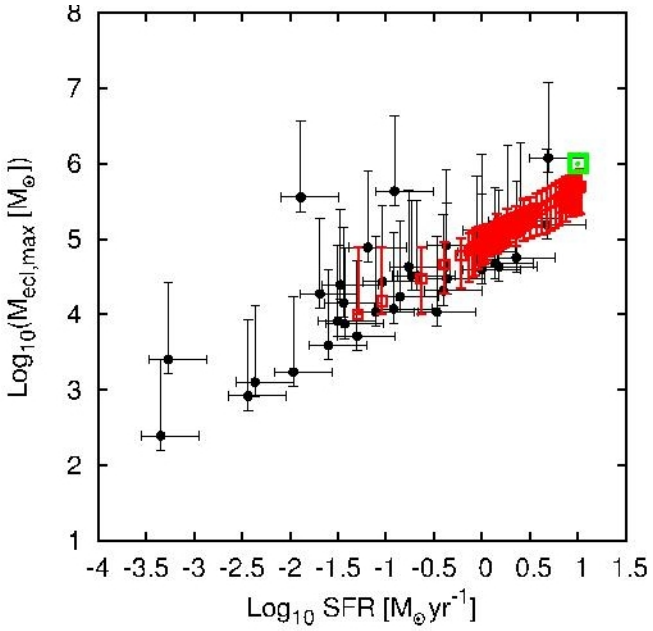

Figure 8. The dependence of the maximum embedded cluster mass on the underlying global SFR of the host galaxy, both in logarithmic units. Red open squares are the calculated M_{ecl}^{max} from vertical stellar velocity dispersion data (Kroupa 2002b). The corresponding SFR for each M_{ecl}^{max} is calculated from the IGIMF theory (Weidner & Kroupa 2004) using Eq. 8. Filled dots are extragalactic observations by Weidner, Kroupa & Larsen (2004) based on data by Larsen (2002). The green symbol is the maximum embedded cluster mass for the thick disk which is assumed to have a mass of $M = 0.2\ M_{disk}$, where $M_{disk} = 5 \times 10^{10} M_{\odot}$. We assume the thick disk formation time scale is 1 Gyr.

- От истории звездообразования зависит не только наклон функции масс СКОПЛЕНИЙ, а еще и верхний предел масс этих самых скоплений…

Подгонка PDMF Scalo (1986)

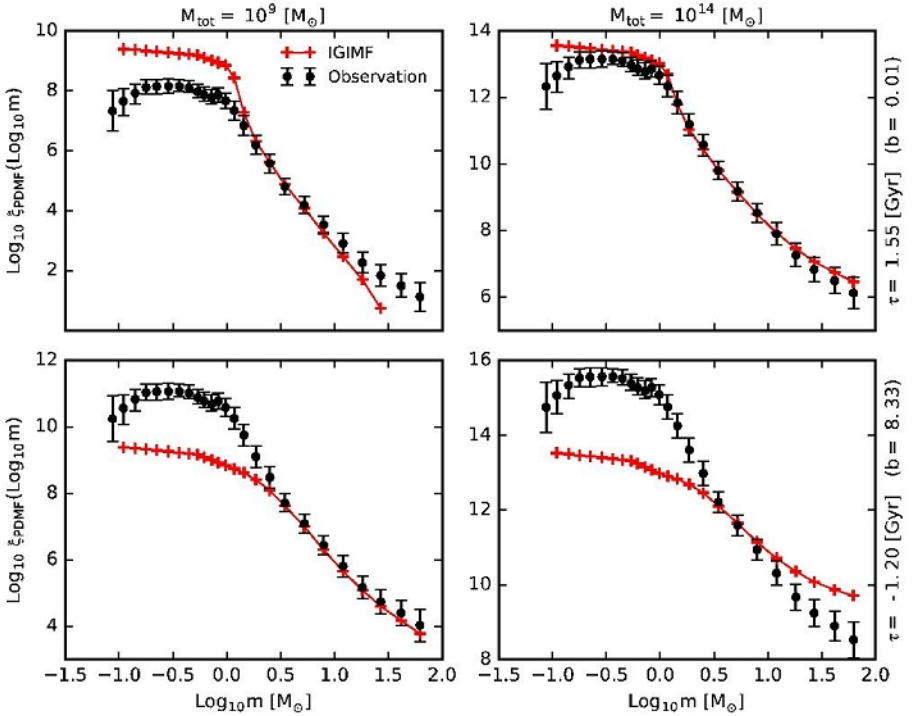

Figure 1. The influence of assuming different values of M_{tot} and τ on the PDMF of the Galaxy is shown by adopting extreme values of M_{tot} (i.e., 10^9 and $10^{14} M_\odot$) and τ (i.e., 1.55 and -1.2 Gyr). Decreasing the total mass of the disk leads to a smaller present-day SFR with a deficiency of massive stars. Exponentially increasing SFRs with negative values of τ lead to a larger $b = \psi_{(t=0)}/<\psi>$ and to a top-heavy IMF (see also Table 1). The solid dots are data from Scalo (1986).

Варьируются 2 параметра истории звездообразования

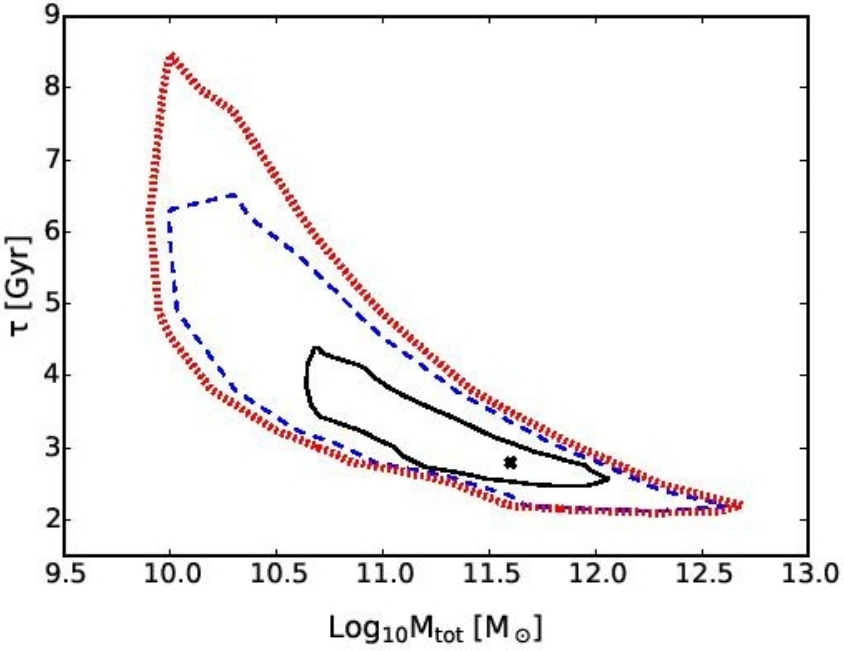

Figure 4. The 0.68%, 0.95% and 0.98% confidence regions for M_{tot} and τ by comparing the IGIMF model with the observed PDMF of the thin disc of the MW. See text and Table 2 for more details.

Хотя вырождение параметров никто не отменял…

Table 2. Details of the best-fitting parameters obtained for the Milky Way thin disk based on different assumptions for the IMF. Columns 2 and 3 give the best-fitting values of Galactic initial parameters, the e-folding time scale and total mass converted into MW-thin-disc stars. Column 4 gives the corresponding χ^2 (Eq. 13). The best-fitting present-day stellar mass-to-light ratio (including remnants), present-day stellar mass, and present-day SFR are given in column 5, 6 and 7, respectively. The last two columns give the number of black holes and neutron stars in the Galactic thin disk for the best-fitting models.

IMF	τ $[Gyr]$	M_{tot} $[10^{11}M_\odot]$	χ^2	M_*/L_V $[M_\odot/L_\odot]$	M_* $[10^{11}M_\odot]$	$\psi_{t=T_G}$ $[M_\odot yr^{-1}]$	N_{BH} $[10^8]$	N_{NS} $[10^8]$
Canonical	$2.8^{+0.5}_{-0.1}$	1.0	1.16	$1.35^{+0.06}_{-0.17}$	0.6 ± 0.01	$1.03^{+0.52}_{-0.08}$	1.0	9.0
IGIMF	$2.8^{+1.7}_{-0.1}$	$4.0^{+8.6}_{-3.5}$	0.88	$2.79^{+0.48}_{-0.38}$	$2.1^{+3.0}_{-1.5}$	$4.1^{+3.1}_{-2.8}$	9.8	47.0
$IGIMF_{\beta 1}$	$2.8^{+1.7}_{-0.1}$	$0.8^{+11.8}_{-0.3}$	0.74	$2.81^{+0.46}_{-0.40}$	$0.45^{+4.6}_{-0.01}$	$0.82^{+6.92}_{-0.1}$	1.51	8.63
$IGIMF_{\beta 2}$	$3.8^{+0.7}_{-1.1}$	$6.0^{+6.6}_{-5.5}$	1.29	$1.38^{+1.9}_{-0.1}$	$3.7^{+1.4}_{-3.1}$	$12.2^{+0.1}_{-10.9}$	8.68	52.10
constrained SFH								
Canonical	$4.9^{+0.7}_{-1.1}$	1.0	9.46	$0.87^{+1.15}_{-0.32}$	$0.6^{+0.01}_{-0.01}$	$3.05^{+0.02}_{-0.62}$	1.13	8.81
IGIMF	$4.9^{+0.7}_{-1.1}$	$0.50^{+11.6}_{-0.08}$	3.92	$1.87^{+0.85}_{-0.03}$	$0.31^{+1.07}_{-0.01}$	$1.53^{+5.63}_{-0.27}$	0.59	4.35